Secondary Instabilities and Spatiotemporal Chaos in Parametric Surface Waves

Wenbin Zhang* and Jorge Viñals
Supercomputer Computations Research Institute, Florida State University, Tallahassee, Florida 32306-4052
(Received 22 November 1993)

A 2D model is introduced to study the onset of parametric surface waves, their secondary instabilities, and the transition to spatiotemporal chaos. We obtain the stability boundary of a periodic standing wave above onset against Eckhaus, zigzag, and transverse amplitude modulations (TAM), as a function of the control parameter ε and the wavelength of the pattern. The Eckhaus and TAM boundaries cross at a finite value of ε, thus explaining the finite threshold for the TAM observed experimentally. At larger values of ε, a numerical solution reveals a transition to spatiotemporal chaotic states mediated by the TAM instability.

PACS numbers: 47.52.+j, 47.35.+i, 47.54.+r

A layer of incompressible fluid that is driven by a sinusoidal force normal to the free surface at rest exhibits parametrically excited surface waves, also known as Faraday waves [1,2]. We introduce in this paper a two-dimensional model that possesses many of the features observed in experimental studies of Faraday waves in low viscosity fluids: a primary instability to a standing wave pattern, a secondary instability (transverse amplitude modulation or TAM) at larger amplitudes of the dimensionless driving force ε, and a chaotic state at yet larger values of ε. Our study focuses on the large aspect ratio limit in which the wavelength of the wave is much smaller than the lateral dimension of the fluid layer.

Recent experiments on Faraday waves in large aspect ratio systems have revealed a number of interesting phenomena [3–8]. Among them, periodic standing wave patterns near onset are found to be unstable against a TAM at some finite supercriticality [3,4,6]. Associated with this instability, temporal fluctuations of the pattern have been observed, with a characteristic time scale that decreases continuously with increasing ε. Beyond a certain value of ε, the wave patterns appear temporally chaotic and spatially disordered [3,4,6,7]. The origin of the TAM instability and its relationship with the disordered state was first studied theoretically by Ezerskii *et al.* [4], who derived a one-dimensional model to describe the modulation. Later, Milner [9] derived a set of coupled amplitude equations for a two-dimensional surface, including the nonlinear interaction and damping of the waves. He showed that a pattern of square symmetry is realized near onset in fluids of low viscosity, and that it can become unstable against a TAM. However, its finite threshold and the issue of wave-number selection remain not well understood [2]. Studies of chaotic wave patterns were also conducted by Rabinovich, Reutov, and Rogal'skii [10], who numerically studied an amplitude equation for a pair of counterpropagating waves, and found features similar to the chaotic states observed in the experiments.

To address the issues of pattern selection and the transition to a disordered state we have derived a set of quasipotential equations (QPEs), valid for weakly damped surface waves [11]. Following earlier work of Lundgren and Mansour on free surface waves [12], we have derived the QPEs from the Navier-Stokes equations by performing a perturbation expansion in the small thickness of the viscous boundary layer at the fluid surface. The QPEs have been further expanded up to third order in the wave steepness to yield a closed set of (nonlocal) equations involving only the free surface displacement from planarity and the velocity potential on the surface. These equations have been used as a starting point for a multiscale asymptotic analysis to obtain amplitude and envelope equations valid near onset, and based on these amplitude equations the symmetry of the selected pattern of standing waves is determined [11]. Because of the complicated nonlinear terms in the QPEs, it is difficult to study analytically secondary instabilities of the base pattern and the possible mechanism responsible for the onset of spatiotemporal chaos observed experimentally. In order to make further progress in this direction we introduce in this paper a simplified model [defined in Eq. (1) below] that retains the rotational symmetry of the fluid layer and many of the qualitative features of the original model, but that incorporates only the simplest possible functional form of the nonlinear terms. The main difference between Eq. (1) and the full model is that the primary instability in the former leads to a standing pattern of lines (one-dimensional periodic solutions), instead of a pattern of square symmetry in the latter. On the other hand, the amplitude equation associated with Eq. (1) reduces to Milner's amplitude equations when ψ is assumed to be modulated along particular directions of propagation, and to Ezerskii *et al.* one-dimensional equation in the case they considered. We therefore expect that our findings concerning secondary instabilities, and the general features of the transition to spatiotemporal chaos, are qualitatively similar to the more realistic case in which the standing wave pattern near onset exhibits square symmetry. We first obtain the stability boundaries of the line pattern for either phase (Eckhaus and zigzag) or amplitude (TAM) instabilities. Numerical integration is then

 0031-9007/95/74(5)/690(4)$06.00

used to study pattern selection above onset, and a transition to spatiotemporal chaotic states mediated by a TAM at finite ε.

The model equation that we study in this paper is

$$\partial_t \psi = -\gamma\psi + if\psi^* + \frac{3i}{4}(1+\nabla^2)\psi + (i-\gamma_n)|\psi|^2\psi, \tag{1}$$

where $\psi(x,y,t)$ is a two-dimensional complex field. The fluid surface displacement from planarity $h(x,y,t)$ and the velocity potential at the free surface $\phi(x,y,t)$ can be expressed in terms of $\psi(x,y,t)$ as $h = \exp(-i\Omega t/2)\psi +$ c.c., and $\phi = -i\exp(-i\Omega t/2)\psi +$ c.c., respectively [11,13]. Ω is the angular frequency of the externally imposed sinusoidal acceleration $f_0\cos(\Omega t)$, with f_0 its amplitude. Equation (1) has been made dimensionless by choosing $2/\Omega$ as a unit of time and $1/q_0$ as a unit of length. The critical wave number q_0 at onset is determined by the condition for subharmonic resonance, $\Omega/2 = \omega(q_0)$, where $\omega(q)$ is the linear dispersion relation of surface waves [for capillary waves, $\omega^2(q) = \Gamma q^3/\rho$, where Γ is the surface tension and ρ the fluid density]. The linear damping coefficient $\gamma = 4\nu q_0^2/\Omega$ [$= \nu(4\rho^2\Omega/\Gamma^2)^{1/3}$ for capillary waves], with ν the kinematic viscosity of the fluid. The nonlinear damping coefficient γ_n is of the order of γ, but, at the level of this simplified model, it has to be considered phenomenological [Eq. (1)]. The quantity $\varepsilon = (f-\gamma)/\gamma$ is the distance away from threshold of the primary instability, where $f = f_0 q_0/\Omega^2$ is the dimensionless driving amplitude.

The quiescent solution $\psi = 0$ becomes linearly unstable against a periodic perturbation of wave number q for $\varepsilon > \varepsilon_c(q) = \sqrt{1 + [3(1-q^2)/4\gamma]^2} - 1$. The curve $\varepsilon = \varepsilon_c(q)$ is the neutral stability curve that separates the region of stability [$\varepsilon < \varepsilon_c(q)$] from the region of instability [$\varepsilon > \varepsilon_c(q)$]. Given a wave number q, Eq. (1) has an unstable (growing) linear eigenmode and a stable (decaying) linear eigenmode with eigenvalues $\lambda_\pm = -\gamma \pm \sqrt{f^2 - [3(1-q^2)/4]^2}$, respectively. The mode $q = 1$ is critical at onset [$\varepsilon_c(q=1) = 0$], which corresponds to the onset of subharmonic resonance of Faraday waves. For $\varepsilon > 0$, stationary line solutions can be approximately found by considering a one-mode Galerkin approximation $\psi_0(x,q) = \alpha_q e^{i\theta_q}\cos(qx) + \mathcal{O}(\alpha_q^3)$ with

$$\alpha_q^2 = \frac{q^2 - 1 - 4\gamma\gamma_n/3 + \sqrt{(q^2-1-4\gamma\gamma_n/3)^2 + (1+\gamma_n^2)[16(f^2-\gamma^2)/9 - (q^2-1)^2]}}{1+\gamma_n^2},$$

$\sin 2\theta_q = (\gamma + 3\gamma_n\alpha_q^2/4)/f$, and $\cos 2\theta_q = \frac{3}{4}(q^2 - 1 - \alpha_q^2)/f$. Another solution, which does not exist for $q = 1$ and is unstable with respect to uniform amplitude perturbations, will not be considered here. We have studied its linear stability against long wavelength phase modulations of the line solution: $\psi(x,y,t) = \psi_0(x,q) + a(x,y,t)\partial\psi_0/\partial x$. We find an Eckhaus stability boundary given by

$$3(\alpha_q^2 + 1 - q^2)\left(\frac{2}{3}\alpha_q^2 + 1 - q^2\right)\left(q^2 + \frac{\alpha_q^2}{2}\right) = 2\gamma_n q^2\alpha_q^2(2\gamma + \gamma_n q^2) - \gamma_n q^2\left(2\gamma + \frac{3}{2}\gamma_n q^2\right)\left(\frac{2}{3}\alpha_q^2 + 1 - q^2\right), \tag{2}$$

and a region of instability against zigzag perturbations given by $\alpha_q^2 < \frac{3}{2}(q^2-1)$ [11]. Figure 1 shows the Eckhaus and zigzag stability boundaries for $\gamma = 0.1$ (experiments on low viscosity fluids have been performed in the range $\gamma = 0.05 - 0.07$ [3], and for $\gamma = 0.07$ [4]) and $\gamma_n = 0.05$. The reentrant shape of the Eckhaus boundary is a direct consequence of the existence of a small nonlinear damping coefficient γ_n. In the limit of small ε ($\varepsilon \ll \gamma_n^2$), the Eckhaus boundary is symmetric around $q = 1$, and is given by $\varepsilon = (27/32\gamma^2)(1-q^2)^2$, whereas, for $\gamma_n = 0$, the stable region is $\varepsilon < \sqrt{1 + [3(1-q^2)/8\gamma]^2} - 1$ and $q \geq 1$, which lies entirely in the region $q > 1$. The parabolic stability boundary for $\varepsilon \ll \gamma_n^2$ ($\gamma_n \neq 0$) can also be obtained from a stability analysis of a standing wave amplitude equation, obtained by assuming that the amplitude of the decaying linear eigenmode of Eq. (1) adiabatically follows the growing eigenmode in Eq. (1), in analogy with Milner's calculation [9]. This approximation, however, fails to reproduce Eq. (2) for larger values of ε.

It is useful at this point to discuss why the order parameter ψ in Eq. (1) is complex. Very close to the primary instability ($\varepsilon = 0$), it is possible to obtain a reduction to a real order parameter equation that corresponds to a standing wave amplitude equation. However, as a result of the small viscosity limit studied, the linearly stable mode of Eq. (1) is only very weakly damped ($|\lambda_-| \ll 1$), and its dynamics may remain important for $\varepsilon > 0$. This is indicated by the fact that the Eckhaus stability boundary [calculated from Eq. (1)] and that given by a standing wave amplitude equation only agree for $\varepsilon \ll \gamma_n^2$ (with $\gamma_n \ll 1$). Furthermore, a stability analysis of the line solution based on the standing wave amplitude equation incorrectly shows that this solution is always stable against a TAM [9].

Stability against transverse amplitude modulations can be studied by considering that $\psi(x,y,t) = [1 + a(y,t)]\psi_0(x,q)$, with $a(y,t) = a_0(t)\cos(Qy)$ (Q small) and linearizing the resulting equation for $a(y,t)$. The TAM unstable region is given by

$$\tfrac{3}{16}(q^2-1)^2 > \tfrac{3}{4}\gamma_n^2\alpha_q^4 + \gamma\gamma_n\alpha_q^2, \tag{3}$$

and is shown as the shaded region in Fig. 1. The line solution can be unstable against a TAM of finite wave

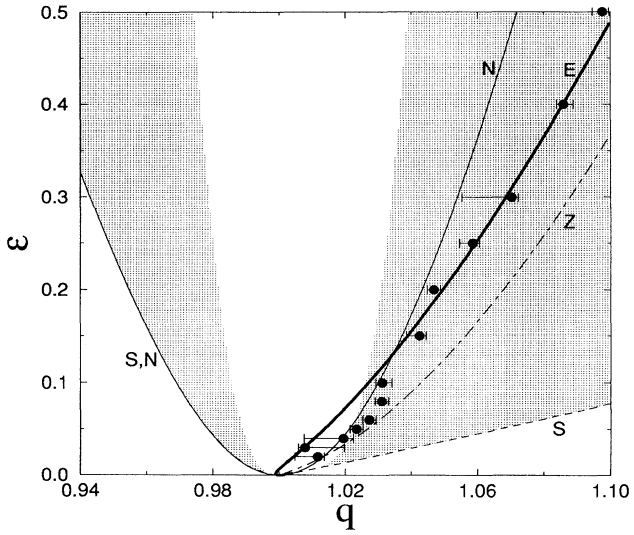

FIG. 1. Stability diagram for $\gamma = 0.1$ and $\gamma_{n=0.05}$ in the (q, ε) plane: boundary of existence of stationary line solutions (dashed line, S). For $q > \sqrt{1 + 4\gamma\gamma_n/3}$ the bifurcation is subcritical, and this portion of the line S corresponds to a saddle node bifurcation; $q_{\max}$, the peak of the azimuthally averaged structure factor calculated numerically (circles with error bars indicating the half width at half maximum of the peak); neutral stability curve (thin solid line, N); Eckhaus stability boundary (thick solid line, E); zigzag stability boundary (long-dashed line, Z). The TAM unstable region is the shaded area.

number Q, but it is always stable against a TAM of wave number $Q \to 0$. Thus, the TAM instability is an amplitude instability [14]. If $\gamma_n = 0$, *all* line solutions are unstable to TAM. If, on the other hand, $\gamma_n \neq 0$, a region of wave numbers around $q = 1$ is stable. At fixed γ, increasing γ_n increases the width of this stable region. For finite γ_n, the Eckhaus and TAM stability boundaries cross at $\varepsilon = \varepsilon_\times(\gamma_n)$ ($\varepsilon_\times \approx 0.1$ for $\gamma_n = 0.05$ in Fig. 1). For $\varepsilon < \varepsilon_\times$, there is a region of stability for the stationary line state against both Eckhaus and TAM perturbations (although it is possibly unstable against zigzag perturbations). As ε is increased away from threshold, the band of stable states shifts toward the region $q > 1$, and for $\varepsilon > \varepsilon_\times$ all solutions that are within the Eckhaus stability boundary lose stability against a TAM. Therefore the reentrant shape of the Eckhaus boundary, and the fact that it crosses the TAM boundary at $\varepsilon = \varepsilon_\times(\gamma_n)$, provides a mechanism for a finite threshold for the TAM instability.

We next turn to the results of our numerical calculation. We have used a pseudospectral method to solve Eq. (1) on a square grid of size $64\pi \times 64\pi$, with periodic boundary conditions. The number of Fourier modes used for each axis is 256. Time stepping is performed by a Crank-Nicholson scheme for the linear terms (including ψ^*), and a second order Adams-Bashforth scheme for the nonlinear terms. The time step used is $\Delta t = 0.1$. The initial condition $\psi(x, y, t = 0)$ is a set of Gaussianly distributed random numbers, of zero mean and variance 10^{-4}. A typical run length is $10^5 - 10^6$ time steps.

Fourier modes with wave numbers close to $q = 1$ are seen to dominate in the early linear regime. As the system enters the nonlinear regime, the azimuthally averaged structure factor exhibits a dominant peak at $q = q_{\max}(t)$ which is seen to shift away from 1 and toward the Eckhaus stable region for all values of ε, i.e., the dominant wave number of the line pattern shifts to $q > 1$. The asymptotic value of $q_{\max}$ at long times is shown by the circles in Fig. 1. The error bars indicate the half width at half maximum of the peak in the azimuthally averaged structure factor. As predicted by the stability analysis, for sufficiently large values of ε ($\varepsilon \geq 0.05$) $q_{\max}$ enters the TAM unstable region before it can reach the Eckhaus stability boundary.

We finally describe the asymptotic temporal dependence of the configurations as a function of ε. The results reported correspond to $\gamma = 0.1$ and $\gamma_n = 0.05$, but they are qualitatively similar to other cases provided that $\gamma_n \neq 0$ (for larger γ_n, both the appearance of the TAM and the transition to chaotic states are seen at larger ε). An almost perfect and stationary line pattern is found for $\varepsilon = 0.02$ [Fig. 2(a)]. As ε is increased to $\varepsilon = 0.05$ a very slowly varying transverse modulation of the line pattern is observed [Fig. 2(b)]. The wavelength of the modulation is $3.2\lambda_0$, with $\lambda_0 = 2\pi$ the critical

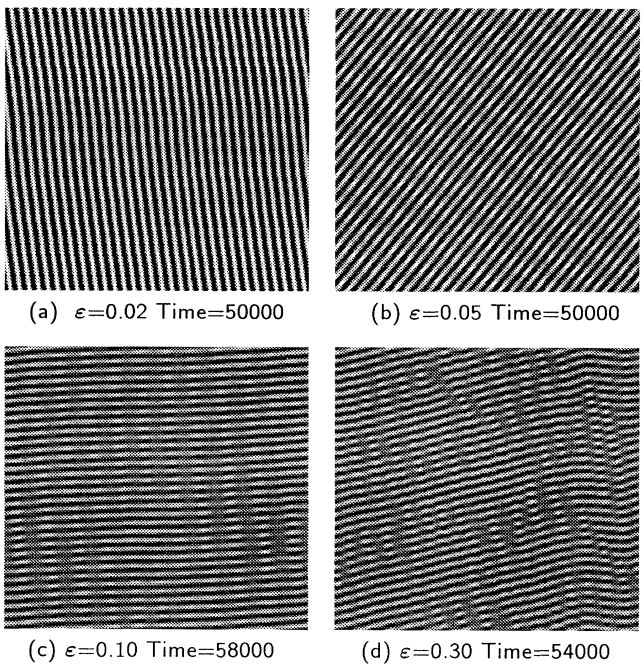

FIG. 2. Typical configurations of $\mathrm{Re}[\psi]$ at long times (shown in gray scale) for four values of ε, starting from a random initial configuration. The configurations of $\mathrm{Im}[\psi]$ are similar. Note that the surface displacement away from planarity is given by $h(x, y, t) = 2(\cos(\Omega t/2)\mathrm{Re}[\psi] + \sin(\Omega t/2)\mathrm{Im}[\psi])$, and that given the isotropy of Eq. (1) any orientation of the pattern is equally likely.

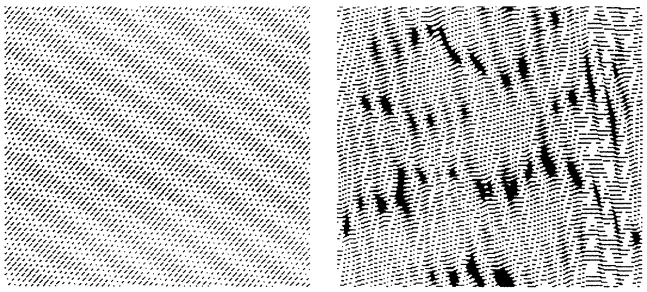

FIG. 3. Zeros of the modulus $\|\psi\|$ ($\|\psi\| < \|\psi\|_{\max}/8$ is considered a zero) for two values of ε and the same configurations shown in Fig. 2.

wavelength at onset. The periodic and almost stationary modulation suggests that the finite amplitude modulated pattern at $\varepsilon = 0.05$ can be described by $\psi(x, y) = A_0[1 + b_0 \cos(Qy)] \cos qx + \cdots$. Figure 3(a) shows the zeros of $\|\psi\|$ ($\|\psi\| < \|\psi\|_{\max}/8$ is considered a zero). They all originate from the $\cos qx$ factor. Hence the TAM is weak enough that $\|1 + b_0 \cos(Qy)\| > 0$. At $\varepsilon = 0.1$ [Fig. 2(c)], the modulation becomes stronger and additional zeros of $\|\psi\|$ appear. We call the regions in which the slowly varying component of $\|\psi\|$ is zero a TAM defect. At this value of ε the wave pattern becomes time dependent, with the temporal variation of the wave pattern coming mostly from the motion of TAM defects. At $\varepsilon = 0.3$ [Fig. 2(d)], the length scale of the modulation becomes smaller, and the density of TAM defects increases [Fig. 3(b)]. The wave pattern can be roughly described as an erratic motion of TAM defects superimposed to an otherwise stationary line state. In order to characterize the temporal fluctuations of the wave patterns in this state, we have calculated the power spectrum of a time

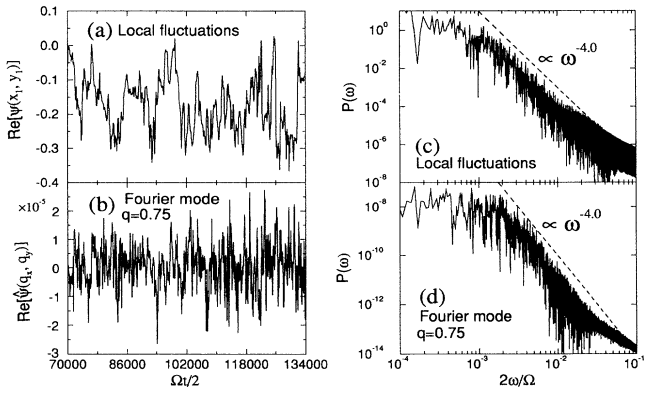

FIG. 4. (a) Time series of $\mathrm{Re}[\psi]$ at a fixed spatial point. (b) Time series of a Fourier mode $\mathrm{Re}\,[\psi(q_x = 0.75, q_y = 0)]$. (c) Power spectrum of the time series shown in (a). (d) Power spectrum of the time series shown in (b). The dashed line represents a power law with an exponent of -4.

series of both ψ at a fixed point in space and the amplitude of a fixed Fourier mode. Figure 4 shows the time series of $\mathrm{Re}[\psi]$ at a fixed point [Fig. 4(a)], and of the Fourier mode $q = 0.75$ [Fig. 4(b)], and their corresponding power spectra [Figs. 4(c) and 4(d)] for $\varepsilon = 0.5$. The power spectra are broadband and decay as a power law of frequency ω^{-z} with $z \approx 4.0$ for frequencies in the range of $2 \times 10^{-3} < 2\omega/\Omega < 2 \times 10^{-2}$. Similar power law decay of the power spectra is also observed for $\varepsilon = 0.3$. The power law decay and the value of the exponent z are in good agreement with experimental results [3].

We wish to thank Maxi San Miguel for many stimulating discussions and for his contributions to the understanding of the stability diagram. This work is supported by the Microgravity Science and Applications Division of the NASA under Contract No. NAG3-1284. This work is also supported in part by the Supercomputer Computations Research Institute, which is partially funded by the U.S. Department of Energy, Contract No. DE-FC05-85ER25000.

*Present address: Department of Chemical Engineering, Massachusetts Institute of Technology, Cambridge, MA 02139.

[1] J. Miles and D. Henderson, Annu. Rev. Fluid Mech. **22**, 143 (1990).
[2] M. C. Cross and P. C. Hohenberg, Rev. Mod. Phys. **65**, 851 (1993).
[3] N. B. Tufillaro, R. Ramshankar, and J. P. Gollub, Phys. Rev. Lett. **62**, 422 (1989); J. P. Gollub and R. Ramshankar, in *New Perspectives in Turbulence,* edited by L. Sirovich (Springer-Verlag, New York, 1991), p. 165.
[4] A. B. Ezerskii, M. I. Rabinovich, V. P. Reutov, and I. M. Starobinets, Zh. Eksp. Teor. Fiz. **91**, 2070 (1986) [Sov. Phys. JETP **64**, 1228 (1986)]; A. B. Ezersky and M. I. Rabinovich, Europhys. Lett. **13**, 243 (1990).
[5] S. Ciliberto, S. Douady, and S. Fauve, Europhys. Lett. **15**, 23 (1991).
[6] B. Christiansen, P. Alstrom, and M. T. Levinsten, Phys. Rev. Lett. **68**, 2157 (1992).
[7] E. Bosch and W. van de Water, Phys. Rev. Lett. **70**, 3420 (1993).
[8] B. J. Gluckman, P. Marcq, J. Bridger, and J. P. Gollub, Phys. Rev. Lett. **71**, 2034 (1993).
[9] S. T. Milner, J. Fluid Mech. **225**, 81 (1991).
[10] M. I. Rabinovich, V. P. Reutov, and A. V. Rogal'skii, Phys. Lett. A **144**, 259 (1990); **170**, 217 (1992).
[11] W. Zhang, Ph.D. thesis, Florida State University, 1994.
[12] T. S. Lundgren and N. N. Mansour, J. Fluid Mech. **194**, 479 (1988).
[13] V. E. Zakharov, Zh. Prikl. Mekh. Tekh. Fiz. **9**, 86 (1968) [J. Appl. Mech. Tech. Phys. **9**, 190 (1968)].
[14] F. H. Busse, Rep. Prog. Phys. **41**, 28 (1978).

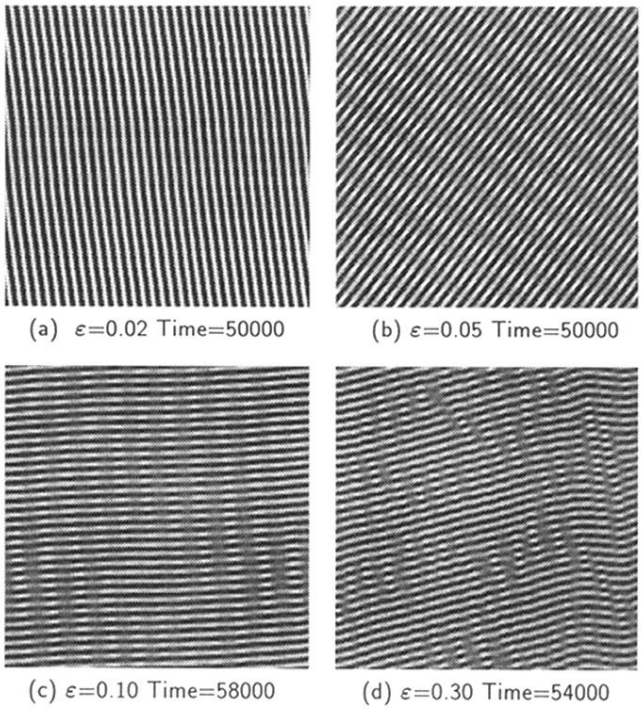

FIG. 2. Typical configurations of $\mathrm{Re}[\psi]$ at long times (shown in gray scale) for four values of ε, starting from a random initial configuration. The configurations of $\mathrm{Im}[\psi]$ are similar. Note that the surface displacement away from planarity is given by $h(x, y, t) = 2(\cos(\Omega t/2)\mathrm{Re}[\psi] + \sin(\Omega t/2)\mathrm{Im}[\psi])$, and that given the isotropy of Eq. (1) any orientation of the pattern is equally likely.